Available online at www.sciencedirect.com
SCIENCE DIRECT®
Talanta 59 (2003) 327–333
Talanta
www.elsevier.com/locate/talanta

Analysis of 2,4,6-trinitrotoluene, pentaerythritol tetranitrate and cyclo-1,3,5-trimethylene-2,4,6-trinitramine using negative corona discharge ion mobility spectrometry

T. Khayamian *, M. Tabrizchi, M.T. Jafari

Department of Chemistry, Isfahan University of Technology, Isfahan 84154, Iran

Received 25 March 2002; received in revised form 20 September 2002; accepted 25 September 2002

Abstract

In this study, the capability of negative corona discharge ion mobility spectrometry (IMS) for quantitative magnitude of several explosives including 2,4,6-trinitrotoluene (TNT), pentaerythritol tetranitrate (PETN) and cyclo-1,3,5-trimethylene-2,4,6-trinitramine (RDX) has been evaluated for the first time. The total current obtained with the negative corona discharge was about 100 times larger than that of IMS based on ^{63}Ni, which results in a lower detection limit and a wider linear dynamic range. The detection limits for PETN, TNT and RDX were 8×10^{-11}, 7×10^{-11} and 3×10^{-10} g, respectively. The calibration plots for these explosives showed linear dynamic ranges of about four orders of magnitude.

Keywords: Negative corona discharge; Explosives; Ion mobility spectrometry

1. Introduction

The analysis of explosive compounds at trace levels is a crucial research field for security purposes. Explosives can be analyzed by a variety of methods such as: HPLC-UV [1,2], GC-ECD [3] and ion mobility spectrometry (IMS) [4–7]. Due to low detection limit, fast response, simplicity, and portability, IMS has been proved to be one of the best methods for the detection of trace levels of explosives [8].

Ionization source is one of the key parts of an IMS instrument. A variety of ionization sources have been used for IMS [8]. Recently, we have investigated the capability of continuous corona discharge as an ionization source for IMS in both positive [9,10] and negative modes [11]. In summary, corona discharge is one of the different varieties of electric discharge. A corona discharge may develop in a strongly non-uniform field that is insufficient for electrical breakdown. This situation arises when the characteristic size of the electrode is much smaller than the interelectrode distance. For example a point-to-plane geometry

* Corresponding author. Tel.: +98-311-3912351; fax: +98-311-3912350
E-mail address: taghi@cc.iut.ac.ir (T. Khayamian).

0039-9140/02/$ - see front matter
PII: S0039-9140(02)00521-0

easily shows a corona discharge when a sufficient voltage is applied to the electrodes. Negative corona occurs when the point electrode is negative with respect to plane electrode. The discharge in pure nitrogen produces a huge number of electrons. However, this high intensity electron source can not be simply used in IMS since introducing any electronegative substance in the corona region immediately results in quenching of the discharge. In this connection, a special IMS cell has been designed and optimized to employ this intense electron source without being disturbed by sample [11]. Electrons can be converted to negative ions via electron attachment reaction with substances possessing electron affinity. In this work, the application of negative corona discharge IMS for analysis of pentaerythritol tetranitrate (PETN), 2,4,6-trinitrotoluene (TNT) and RDX is described.

2. Experimental

2.1. Apparatus

The IMS apparatus with continuous corona discharge as the ionization source has been described previously [10]. The IMS cell was made of a glass tube, 4 cm inner diameter and 19 cm long, on which 15 stainless steel guard rings, located 1 mm from each other, are mounted. The guard rings are connected by a series of resistors to form the electric field. The IMS cell was modified for operation in the negative mode [11]. Schematic diagram of the apparatus is shown in Fig. 1. The counter electrode was made of a 2-mm thick graphite disc with a small hole (1.5 mm) in its center. It was mounted inside the glass tube in front of the needle. Another graphite disc, with the same size and shape as the counter electrode, was mounted parallel to the first disc at a 7-mm distance. A flow of nitrogen was introduced between the two discs to serve as a curtain for separation of discharge and ionization regions. This modification prevents diffusion of sample into the corona discharge region and quenching the source. Nitrogen was used as the drift gas, the carrier gas and also as the curtain gas. The gas was filtered with a 13X molecular sieves (Fluka) trap before it entered the IMS in order to remove water vapor or other contamination. The water content in the gas is expected to be about 10 ppm. The optimum experimental conditions for obtaining the ion mobility spectra of the compounds are shown in Table 1.

2.2. Reagents and chemicals

Commercial-grade PETN, RDX and TNT were obtained from Isfahan Chemical Industries. Stock standard solutions (1000 and 10 000 μg ml^{-1}) of PETN, RDX and TNT were prepared in methyl isobutyl ketone (MIBK, Merck). Working solutions were made by successive dilution of the stock solutions with MIBK. Nitric acid and sodium hydrogen carbonate were of analytical reagent grade from Merck.

2.3. Sample introduction system

The injection port was a T shape union made of brass alloy. The carrier gas passes through the port and carries the analyte vapor to the IMS cell. The injection port was equipped with a heating element and a digital temperature controller (TC14P, Alton-Ray, Tehran). A brass cap, holding a fine nichrome filament, is used to introduce samples. The sample, 10 μl, was placed on the filament and after evaporating the solvent, the cap was inserted into the injection port.

3. Results and discussion

The background spectrum shows a very large peak at zero drift time corresponding to electrons, and two small peaks corresponding to negative ions [11]. The origin of the negative ions was thought to be due to the presence of trace amounts of oxygen in the gas. The total intensity of negative ions in the background spectrum is negligible with respect to the electron intensity. The ion mobility spectrum of PETN is shown in Fig. 2. The reduced mobility values for the peaks labeled P_1, P_2, P_3 and P_4 in Fig. 2 are 1.21, 1.27, 2.47 and 2.73 $cm^2\ V^{-1}\ s^{-1}$, respectively (Table 2). The reduced mobility value for P_3 is very close to the reduced

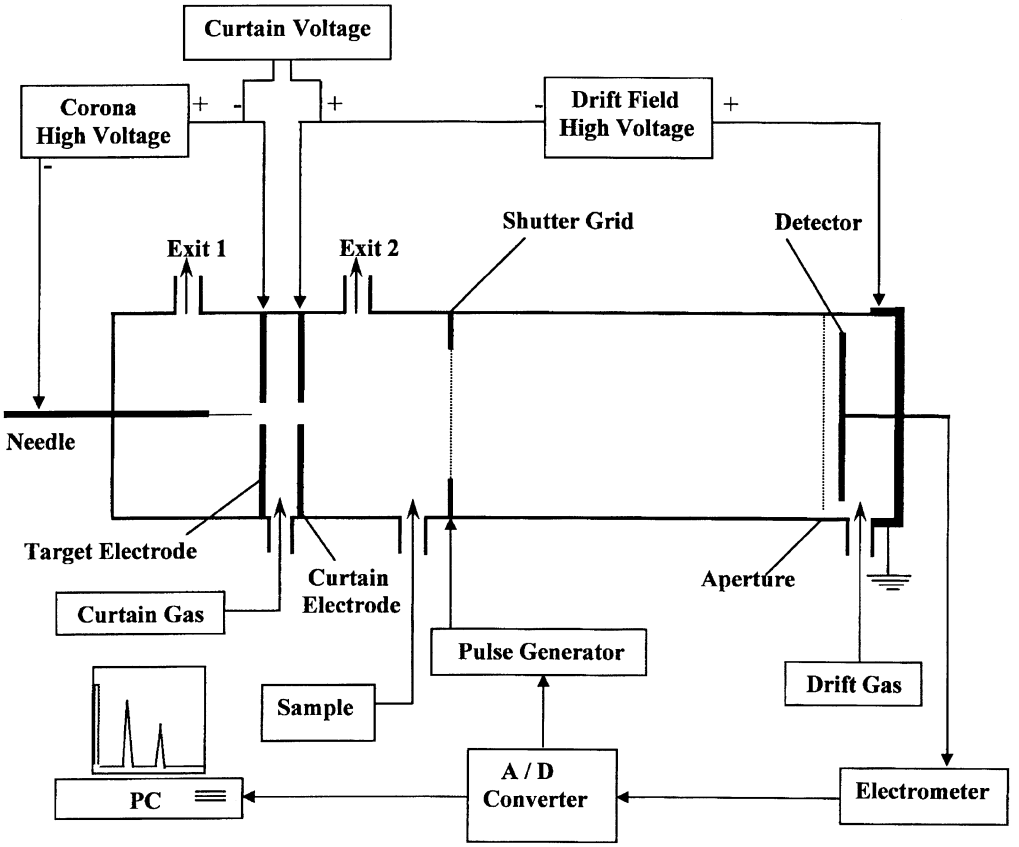

Fig. 1. Schematic diagram of the negative corona discharge ion mobility spectrometer.

Table 1
Optimum experimental conditions

Conditions	PETN	RDX	TNT
Needle voltage (kV)	1.9	1.8	2.2
Drift field (V cm^{-1})	512	450	437
Curtain voltage (kV)	1.0	1.0	1.0
Drift gas flow rate (ml min^{-1})	500	500	500
Carrier gas flow rate (ml min^{-1})	20	20	20
Curtain gas flow rate (ml min^{-1})	80	80	80
Injection port temperature (°C)	165	220	140
Cell temperature (°C)	140	160	170

mobility value of NO_3^- (2.46 and 2.48) reported by Ewing et al. [8]. Rodriguez [12] has pointed out that PETN is fragmented to NO_3^- in a heated IMS drift tube accompanied by an autoionization process to PETN·NO_3^- in nitrogen atmosphere. Eiceman et al. [6] studied the mass spectrum of PETN with thermal electrons. They showed that there are complex ionic species with the largest one being PETN·NO_3^- ion and a significant amount of NO_3^- ions. Therefore, P_1 might be originated from PETN·NO_3^- ions. At high concentrations P_1 increases while the P_3 peak decreases. This behavior supports the assignment of P_1 to the cluster ion PETN·NO_3^-. The reduced mobility of P_2 peak has not been reported by other authors. The P_4 peak is thought to be NO_2^- as its observed reduced mobility is very close to the that of NO_2^- (2.70 and 2.76 $cm^2\,V^{-1}\,s^{-1}$ reported by Spangler and Collins [13] and Carr [14], respectively. The comparison of the reduced mobilities is helpful in assigning the IMS peaks. In fact, the recognition of the ions with confidence requires coupling of IMS with a mass spectrometer.

It was noticed that the peak intensities of PETN were affected by the cell temperature, as shown in

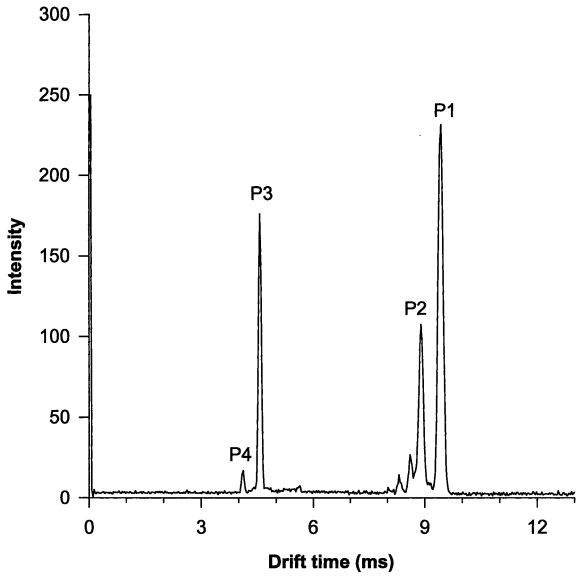

Fig. 2. The ion mobility spectrum of PETN.

Table 2
Characteristic ions for some common explosives

Peak	Reduced mobility (K_o)[a]	Drift time (t)[b]	Temperature (°C)
P_1	1.21 (±0.02)	10.5	140
P_2	1.27 (±0.02)	9.9	140
P_3	2.47 (±0.07)	5.2	140
P_4	2.73 (±0.04)	4.5	140
R_1	1.27 (±0.02)	9.9	160
R_2	1.47 (±0.03)	8.6	160
R_3	2.03 (±0.05)	6.3	160
R_4	2.72 (±0.09)	4.7	160
TNT	1.55 (±0.04)	8.2	170

[a] Reduced mobility values with units of $cm^2\ V^{-1}\ s^{-1}$.
[b] Drift time values with units of ms.

Fig. 3. This Figure shows that increasing the cell temperature enhances the P_3 (NO_3^-) and P_4 (NO_2^-) peaks but depresses the P_1 ($PETN{\cdot}NO_3^-$) and P_2 peaks. This behavior may be attributed to decomposition of PETN to NO_3^- and NO_2^- at elevated temperatures.

The RDX spectrum, at the optimum experimental conditions, is shown in Fig. 4. The reduced mobility for R_4 peak is 2.72 $cm^2\ V^{-1}\ s^{-1}$, which is very close to the reduced mobility value for NO_2^-. The reduced mobility for R_2 peak in Fig. 4 is equal

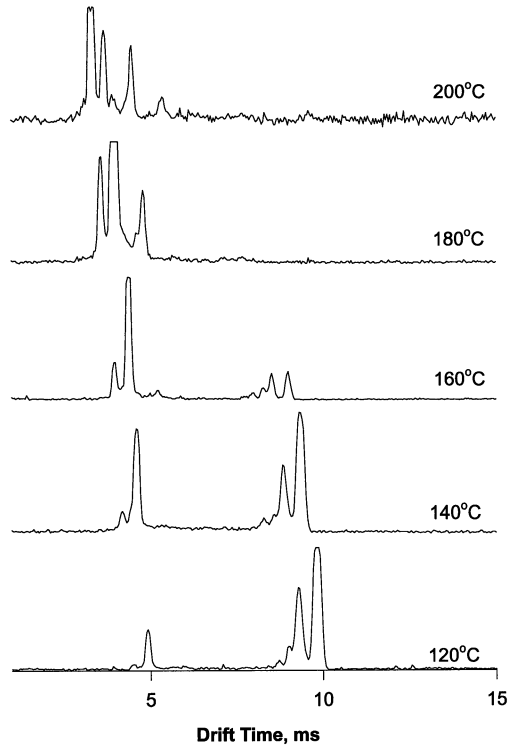

Fig. 3. Spectra of PETN at different drift tube temperatures.

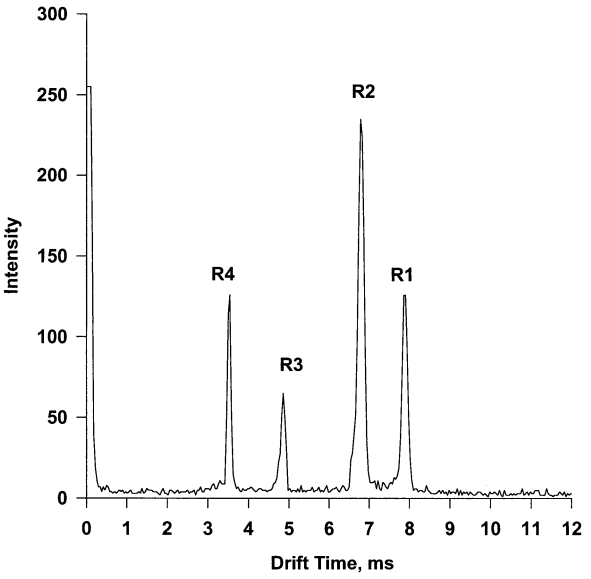

Fig. 4. The ion mobility spectrum of RDX.

to 1.47 $cm^2\,V^{-1}\,s^{-1}$, which is close to the reported reduced mobility value for $M\cdot NO_2^-$ [8].

Fig. 5 shows the effect of the drift tube temperature on the RDX spectrum. It can be observed that as the temperature is elevated, the R_1 and R_2 peak intensities decrease while those of the R_3 and R_4 peaks increase. This behavior might be due to decomposition of the sample at high temperatures. The optimum temperature for RDX is about 150–160 °C.

Ion mobility spectrum of TNT is shown in Fig. 6. The spectrum shows only one peak with the reduced mobility of 1.55. Spangler and Lawless [15] investigated the gas phase chemistry of nitrotoluenes. They found, that, M^- is produced in the absence of a proton abstracting agent. Therefore, the single peak in Fig. 6 could be due to TNT^- ions. This is confirmed by comparison of the reduced mobility of the peak with the reported value for TNT^- (1.49) by Spangler and Lawless [15].

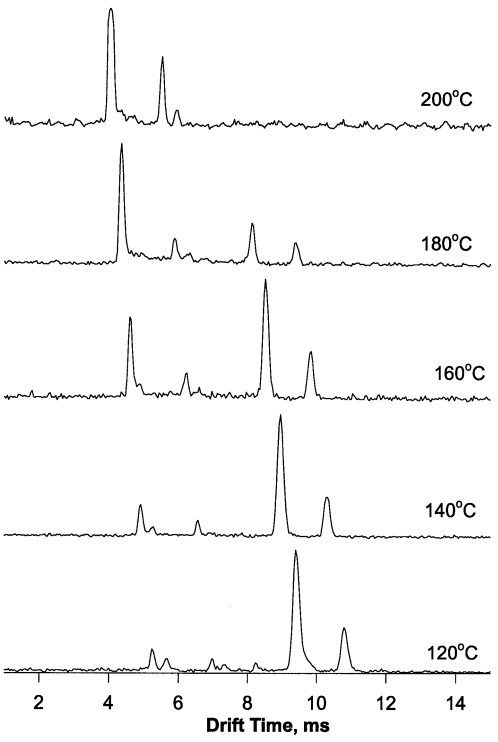

Fig. 5. Spectra of RDX at different drift tube temperatures.

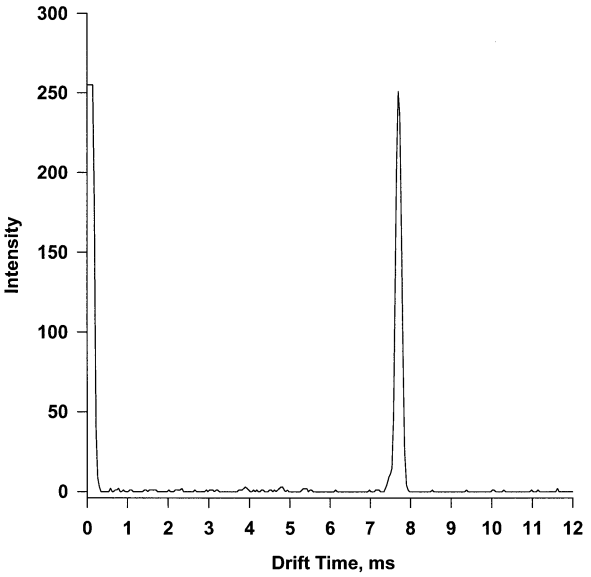

Fig. 6. The ion mobility spectrum of TNT.

In addition to the cell temperature, the injection port temperature also needs to be optimized. The temperature of the injection port affects the amount of vaporized sample and decomposition of the sample. Eiceman et al. [6] showed that at higher temperatures of the injection port, volatilization was accompanied in part by thermal decomposition of the sample. Therefore, the optimization was conducted by considering the sample output from the injection port. This was carried out so that to prevent depletion of electrons and also to keep the response to occur at a suitable acquisition time range. Higher temperature should be prevented to minimize decomposition of the analyte. The optimum injection port temperatures for observing suitable electron and sample peaks and preventing analyte decomposition were about 140, 165, and 220 °C for analysis of TNT, PETN and RDX, respectively.

3.1. Quantitative analysis

3.1.1. Response of the analyte

When the filament, holding the sample, is inserted to the injection port, the signal appears after a short time, reaches a maximum and decays

almost exponentially. It was noticed that during the acquisition time (from the injection time until the sample peaks disappear) the relative peak intensities are changed. Typical behavior of the peak intensities for major ions in the acquisition time is shown in Fig. 7. The area under each peak has been calculated and plotted against the acquisition time. The sum of the peak areas (total) against the acquisition time is also shown in the figure. The integration of this plot was considered as the response.

3.1.2. The changes in peak intensities

Fig. 7 shows that the total peak reaches its maximum gradually, not instantly. This is due to the fact that the desorption of the analyte from the nichrome filament does not occurs instantly. It takes about 6 s that the concentration in the ionization region reaches its maximum level. The total peak then decreases exponentially because of the dilution of the analyte by the carrier gas. At maximum concentration, the $PETN \cdot NO_3^-$ peak (P_1) is maximum while NO_3^- peak (P_3) shows a deep. This behavior may be attributed the formation of $PETN \cdot NO_3^-$ adduct which normally happens at high concentration of sample.

The influence of the sample concentration on each peak may be evaluated by plotting the intensity of each peak versus the total intensities, if the total intensities is assumed to represents the sample concentration. This is shown in Fig. 8 where P_1, P_2, and P_3 are plotted against the sum $(P_1+P_2+P_3)$. As can be seen P_1 always increases with concentration while P_3 at first, increases and then decreases at higher concentration. Such behavior is usually observed for the intermediate species in the consecutive reactions. Therefore the following reactions may be postulated in the ionization region.

$$PETN + e \rightarrow NO_3^-$$

$$NO_3^- + PETN \rightarrow PETN \cdot NO_3^-$$

At low PETN concentration NO_3^- dominates while at high concentration $PETN \cdot NO_3^-$ is the major product ion.

3.1.3. Calibration curves

The response against amount of the explosives was evaluated by plotting the calibration curve. The linear ranges were 3×10^{-10}–1×10^{-6}, 2×10^{-10}–1×10^{-6} and 1×10^{-9}–8×10^{-7} g for PETN, TNT and RDX, respectively. However, the responses were quadratic function from the

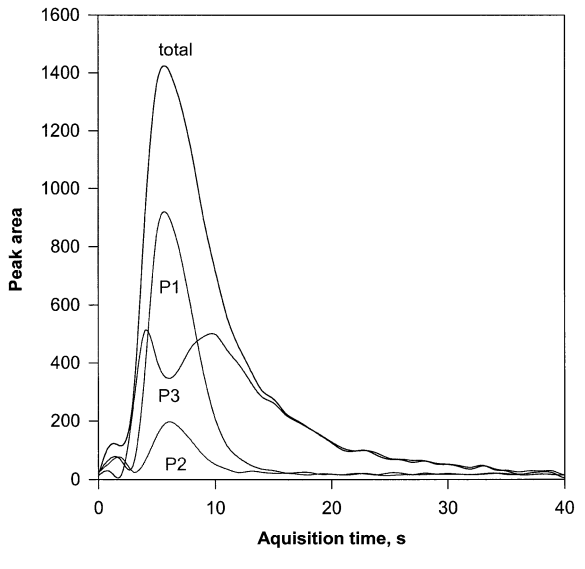

Fig. 7. The areas under the peaks versus the acquisition time.

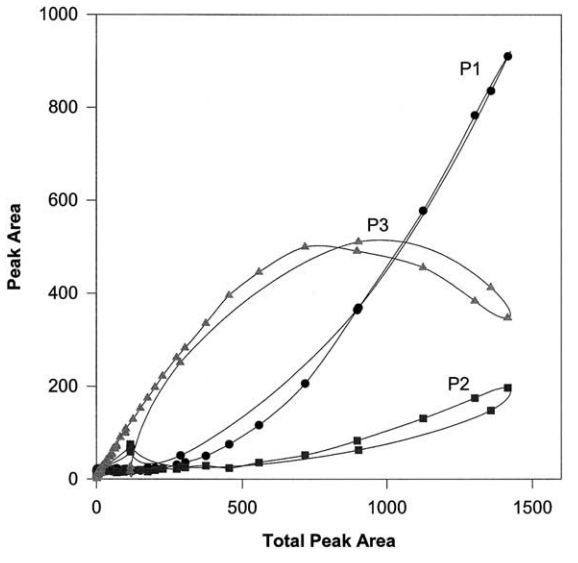

Fig. 8. The plot of peak intensities against the total peak intensity for PETN.

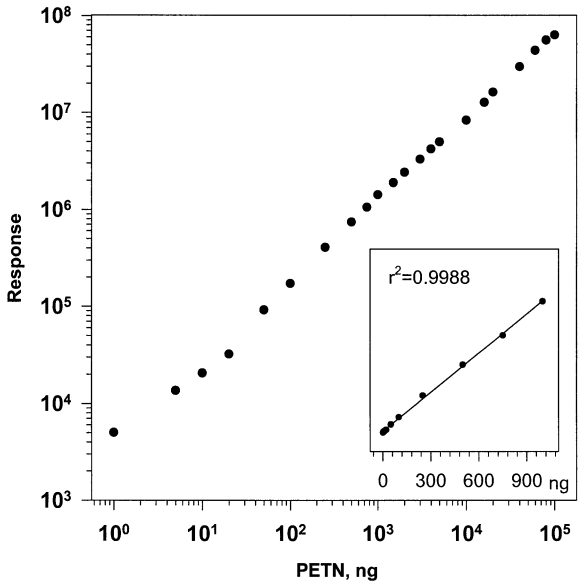

Fig. 9. Plot of IMS response against the amount of PETN, The plot shown as onset of this figure shows the linear section of the calibration curve.

limit of linear response to 1×10^{-4} g of the explosives. The working range and linear dynamic range against mass of PETN is shown in Fig. 9. As can be seen the working range is about five orders of magnitude and the linear dynamic range is about four orders of magnitude. The detection limits were 8×10^{-11}, 7×10^{-11}, and 3×10^{-10} g. for PETN, TNT and RDX, respectively. The minimum detection limits reported by Fetterolf and Clark [4] using ^{63}Ni–IMS were 2×10^{-10} g. for these compounds.

The electron current in negative corona discharge is about 100 times greater than that of ^{63}Ni. The higher current of corona discharge certainly influences the detection limit and the dynamic range. Product ions are formed by the reaction of electrons and analyte. A higher electron density results in more negative ions and consequently a lower detection limit is expected. The dynamic range is also increased because enough electrons are available for ionization at higher concentrations of analyte. The resolving power may also be improved because of the possibility of using narrower injection pulses.

4. Conclusions

The ion mobility spectra of PETN, TNT, and RDX were obtained using negative corona discharge-IMS. The detection limit and the dynamic range of the explosives by negative corona discharge-IMS are superior to that of ^{63}Ni–IMS. The reason is the higher current produced by negative corona discharge. The higher current allows using narrower ion pulse widths. Therefore resolving power may also be increased.

Acknowledgements

The authors acknowledge to the Research Council of Isfahan University of Technology and Center of Excellency in Chemistry of Isfahan University of Technology for the support of this work.

References

[1] F. Garofolo, V. Migliozzi, B. Roio, Rapid Commun. Mass Spectrom. 8 (1994) 527.
[2] C.A. Groom, S. Beaudet, A. Halasz, L. Paquet, J. Hawari, J. Chromatogr. A 909 (2001) 53.
[3] M.E. Walsh, Talanta 54 (2001) 427.
[4] D.D. Fetterolf, T.D. Clark, J. Forensic sci. JFSCA 38 (1993) 28.
[5] J.P. Davies, L.G. Blackwood, S.G. Davis, L.D. Goodrich, R.A. Larson, Anal. Chem. 65 (1993) 3004.
[6] G.A. Eiceman, D. Preston, G. Tiano, J. Rodriguez, J.E. Parmeter, Talanta 45 (1997) 57.
[7] L.M. Matz, P.S. Tornatore, H.H. Hill, Talanta 54 (2001) 171.
[8] R.G. Ewing, D.A. Atkinson, G.A. Eiceman, G.J. Ewing, Talanta 54 (2001) 515.
[9] T. Khayamian, M. Tabrizchi, N. Taj, J. Fresenius, Anal. Chem. 370 (2001) 1114.
[10] M. Tabrizchi, T. Khayamian, N. Taj, Rev. Sci. Instr. 71 (2000) 2321.
[11] M. Tabrizchi, A. Abedi, Int. J. Mass Spectrom. 218 (2002) 75.
[12] J.E. Rodriguez, Master Thesis, New Mexico State University, Las Cruces, NM, 1996.
[13] G.E. Spangler, C.l. Collins, Anal. Chem. 47 (1975) 393.
[14] T.W. Carr, Anal. Chem. 51 (1979) 705.
[15] G.E. Spangler, P.A. Lawless, Anal. Chem. 50 (1978) 884.